Multidisciplinary Journal of Science Technology Education and Management
Journal homepage: http://www.mjstem.org

Bifunctional NiO/Al_2O_3–Catalyzed Conversion of Hemicellulose Extracted from Maize Cobs to Liquid Hydrocarbons

Gambo Muhammad[1*], M. N. Almustapha[2], M. G. Liman[2], Abubakar Aji[3,4], Hauwa Muhammad Abba[5], Mysara Eissa Mohyaldinn[3,7], Hisham Khaled Ben Mahmud[6]

[1]Department of Pure and Applied Chemistry, University of Maiduguri, Bama Road, Maiduguri, Borno State, Nigeria.
[2]Department of Energy and Applied Chemistry, Usmanu Danfodiyo University, Sokoto, Sokoto State, Nigeria.
[3]Department of Petroleum Engineering, Universiti Teknologi PETRONAS (UTP), 32610 Seri Iskandar, Perak Darul Ridzuan, Malaysia,
[4] Nile University of Nigeria, Abuja, Nigeria,
[5]Faculty of Education, University of Maiduguri, Bama Road, Maiduguri, Borno State, Nigeria.
[6]Faculty of Engineering, Sohar University, Oman.
[7]Center of Flow Assurance, Institute of Sustainable Energy & Resources, Universiti Teknologi PETRONAS (UTP), 32610 Seri Iskandar, Perak Darul Ridzuan, Malaysia

*Corresponding Author: Gambo Muhammad (gambomuhammad087@gmail.com, abbakaraji@gmail.com)

Abstract

The growing imperative for sustainable energy sources has spurred significant interest in the catalytic conversion of biomass, such as agricultural waste, into biofuels. Lignocellulosic biomass is a promising raw material for the production of energy and bio-based chemicals. This study investigates the catalytic conversion of hemicellulose derived from maize cobs into liquid hydrocarbons using NiO/Al_2O_3 as a bifunctional catalyst in an aqueous phase. The process comprises the initial generation of furfural via a one-step acid-catalyzed hydrolysis-dehydration sequence, followed by its transformation into liquid hydrocarbons via aldol condensation and hydrodeoxygenation. The empirical results demonstrate a conversion efficiency of 61.08% with the NiO/Al_2O_3 catalyst under optimized reaction conditions (220°C, 30 bar, 1 h), corresponding to a hydrocarbon selectivity of 61.08%. Gas chromatography/mass spectrometry (GC/MS) analysis of the liquid product identified the presence of alkanes within the C_7-C_{15} range, with heptane (28.06%) and decane (17.65%) constituting the principal products. This finding substantiates the viability of employing hemicellulose sourced from maize cobs as a feedstock for producing liquid hydrocarbons through hydrodeoxygenation catalyzed by NiO/Al_2O_3.

Keywords: Bifunctional catalyst, Hydrodeoxygenation catalyst, Initial furfural production, Liquid hydrocarbon, Maize cobs, Sustainable energy sources

Received August 26, 2025 Revised January 02, 2026 Accepted February 19, 2026
EISSN: 3121-9292
ISSN: 3121-6552

1. Introduction

Investment in sustainable energy in the oil and gas sector has increased steadily (Yurukcu et al., 2023) due to frequent crises in the petroleum supply, the risk of scarcity, price volatility, and environmental impacts (Aji et al., 2025a). Interest in alternative energy sources has increased over the last two decades (Biswas et al., 2022; Pustějovská et al., 2023). Currently, the dominant energy resource is fossil fuels. As of 2020, fossil fuel consumption was high, while renewable energy use was very limited, with hydro, wind, solar, and nuclear sources contributing 83%, 12.6%, and 6.3%, respectively (Holechek et al., 2022), while in India, fossil fuels account for over 70% (Channi, 2022). The adverse impacts of fossil fuels, particularly their effects on ecosystems, have underscored the urgent need to transition to sustainable energy sources, which are vital to meeting our energy requirements (Halkos & Gkampoura, 2023). Renewable energy sources are a sustainable and healthier option compared to fossil fuels, offering advantages for human well-being, slowing climate change, and protecting ecosystems (Kandpal & Singh, 2022). Additionally, the combustion of fossil fuels emits CO_2, causing detrimental environmental effects and accelerating the greenhouse effect (Kashef et al., 2022) and global warming (Azni et al., 2023).

Interest in the catalytic conversion of biomass, particularly agricultural waste, into biofuel has increased due to the growing need for sustainable energy alternatives (Inyang et al., 2022). Among biomass resources, agricultural residues, such as maize cobs, are particularly attractive due to their availability and low cost. The literature shows that catalytic conversion of Hemicellulose, a significant component of lignocellulosic biomass, yields valuable liquid hydrocarbons (Aji et al., 2022; Nikolopoulos et al., 2023). Hydrolysis of agricultural residues, such as maize cobs, into ester fuels reduces greenhouse gas emissions and improves environmental performance (Aji et al., 2025b; Qu et al., 2023). These materials can be combusted in boilers to generate heat, which is then converted into electricity (Boni et al., 2023). Bio-waste and residue conversion techniques have enormous potential, both environmentally and economically, owing to the carbon cycle of biomass and technological advancements (Chen et al., 2023). It is also well established that biomass is a safe energy source and can reduce emissions of hazardous gases (Kalak, 2023).

The conversion of lignocellulosic biomass typically proceeds through a multistep catalytic pathway (Figure 1), involving the initial breakdown of hemicellulose into intermediates such as furfural, followed by upgrading to long-chain hydrocarbons via aldol condensation and hydrodeoxygenation (HDO). Numerous studies have explored different catalyst-feedstock combinations for this process. For instance, high hydrocarbon yields have been reported using Ni/Al_2O_3 on food waste (59.48%) (Valizadeh et al., 2020), and $Mo\text{-}Co/\gamma\text{-}Al_2O_3$ on waste cottonseed oil (61.9%) (Melo et al., 2021), while $Pt\text{-}Ni/\gamma\text{-}Al_2O_3$ has been used with pine sawdust (52.67%) (Zheng et al., 2021).

https://doi.org/10.5281/zenodo.18727508

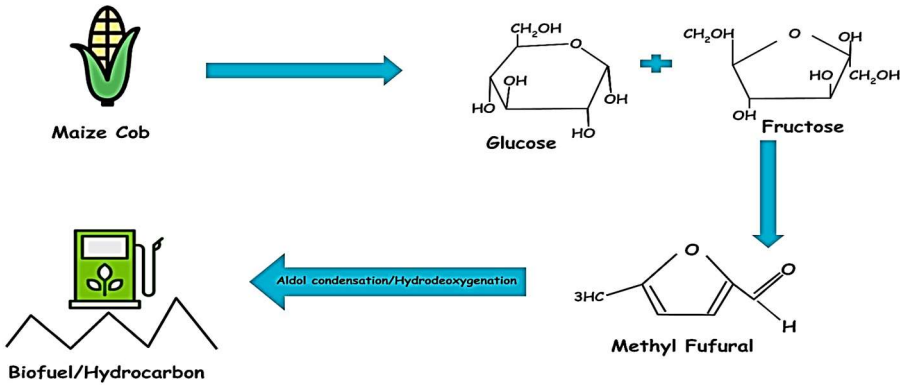

Figure 1: Flow mechanism of hydrocarbon production from Maize cobs

A major challenge in this area is the continued need to enhance the conversion process. This requires the use of cost-effective, highly efficient, and selective bifunctional catalysts capable of processing non-food-competing lignocellulosic feedstocks. In this context, Nickel Oxide supported on Alumina (NiO/Al_2O_3) is a promising candidate. It is a well-established bifunctional catalyst in which the acidic sites of Al_2O_3 facilitate the initial condensation/dehydration reactions, and the nickel-based sites are highly effective for the subsequent hydrogenation and hydrodeoxygenation steps required for alkane production. The selection of this specific catalyst is therefore motivated by its potential for synergistic action of the metallic and acidic sites to achieve high conversion and selectivity from the abundant hemicellulose in maize cobs.

The pressing need for sustainable production of fuels and chemicals without impacting the food supply has driven researchers worldwide to develop second-generation technologies. These technologies aim to use non-edible feedstocks, such as lignocellulosic biomass, while ensuring that food production remains unaffected. Production of liquid fuels via aqueous-phase processing could be a promising approach to harnessing biomass for fuel generation. The process is viable as it uses water-soluble feedstock at moderate temperatures and pressures (Azman et al., 2023). This research aims to convert hemicellulose from maize cobs using NiO/Al_2O_3 as a catalyst. The study employs a systematic approach to investigate catalyst performance by GC/MS, FT-IR, and XRD.

2. Methodology

2.1 Materials

The reagents used in this research were Nickel (II) nitrate, alumina powder, maize cob, sodium chloride (NaCl), sulfuric acid (H_2SO_4), Sodium Sulphate, Acetone, Ethanol (50.0%), and Ethyl acetate.

2.2 Collection and Processing of Samples

Maize cobs were obtained from a processing facility situated in the Nguru Local Government Area of Yobe State, Nigeria. For sample preparation, the cobs were first shade-dried, then ground, and subsequently sieved. The prepared sample was stored in a dry storage area until needed.

2.3 Catalyst Preparation

The Nickel(II) nitrate catalyst was synthesized via the incipient wetness impregnation method, following the procedures outlined by Mathew et al. (2023) and Mo et al. (2023) (Mathew et al., 2023; Mo et al., 2023). This involved adding 100 cm^3 of a 0.6 M Nickel(II) nitrate solution to 200 g of alumina powder (Al_2O_3) at a 1:2 ratio, with constant agitation on a magnetic stirrer. The resulting slurry was subsequently dried at 80 °C for 8 hours. Following drying, the material was calcined at 600 °C for 4 hours. The catalyst was then kept in a desiccator for subsequent characterization and analysis.

2.4 Conversion Process

In the initial reaction steps, glucose and fructose were hydrolyzed. The molecules were converted to methyl furfural and acid catalysts via dehydration. The intermediate was converted to liquid alkanes via aldol condensation and hydrogenation over a bifunctional catalyst at 220 °C reaction temperature and 30 bar for 60 minutes (Jiang et al., 2023).

2.5 Furfurals production

The method outlined by Aji et al. (2022) was adopted for furfural production. The procedure involved first combining 5.0 g of a dried sample with 5.0 g of NaCl in a clean beaker. This mixture was then transferred into a 250 cm^3 borosilicate glass tube reactor. Subsequently, 50 mL of 10% H_2SO_4 was introduced into the reactor. The distillation process was carried out in a furnace, with the reactor positioned upright and connected to a water condenser. Pre-determined variables for acid concentration, temperature, and duration governed the distillation. Following distillation, the organic component of the distillate was extracted with dichloromethane in a separating funnel. Residual water was removed from the extract by adding 0.2 g of sodium sulfate. Finally, the solvent was evaporated at 40°C using a rotary evaporator.

2.6 Aldol condensation

The aldol condensation was performed according to the established methodology described by Aji et al., (2022); Garba et al., (2018). The reaction was conducted in a 250 cm^3 flat-bottomed flask reactor equipped with a magnetic stirrer, employing acetone as a reactant. A reaction mixture was initially prepared, comprising 10 cm^3 of distilled furfural and 5 cm^3 of acetone, maintaining a 2:1 ratio. This was followed by the addition of 50% aqueous ethanol to the mixture. The reactor was subsequently heated to 85°C, and the contents were vigorously stirred at 500 rpm for 30 minutes, during which 20 cm3 of 4 M NaOH was added. Post-reaction workup involved filtration to ensure the complete removal of excess NaOH. This was achieved by triple-washing the mixture with ethanol. Finally, the resulting crystalline product was dissolved in ethyl acetate and analyzed by FTIR.

https://doi.org/10.5281/zenodo.18727508

2.7 Hydrodeoxygenation

Hydrodeoxygenation (HDO) was conducted according to the process described by Aji et al., (2022); Garba et al., (2018). The aldol product was HDO in a stainless-steel tubular reactor. The reaction mixture, composed of 30 cm^3 of the aldol adduct and 1.8 g of NiO/Al_2O_3 catalyst, was subjected to a hydrogen pressure of 30 bar. The reactor was maintained at 220 °C for one hour under an inert atmosphere. Following the reaction, the liquid product was filtered and analyzed by GC-MS.

2.8 XRD and FT-IR Spectroscopic Analyses

XRD of the synthesized catalyst was conducted at the National Geosciences Research Laboratory, Nigerian Geological Survey Agency, Kaduna, Nigeria, utilizing an Empyrean intelligent diffractometer (Malvern Panalytical, Netherlands).

FT-IR spectroscopic analysis was performed on the prepared catalyst, standard furfural, and the furfural aldol adduct. This was carried out at the Central Advanced Science Laboratory Complex, Usmanu Danfodiyo University, Sokoto, using an Agilent Model 650. For the analysis, the sample was combined with the alkali halide potassium bromide (KBr) and compressed into a thin, transparent pellet using a hydraulic press. Spectral data were then recorded with the pellet placed in the spectrometer's standard sample compartment. The transmission rate was measured across the range 4000–650 cm^{-1} with a resolution of 4 (Aji et al., 2022).

2.9 GC-MS Method of Analysis

Analysis of the hydrodeoxygenation product was performed using an Agilent 7890B GC/MS system coupled to an MSD 5977A at the Chemistry Central Laboratory, Yobe State University, Damaturu. The system used a capillary column (30.0 m in length, 250 μm in diameter, 0.25 μm in film thickness). A 1 μL injection volume was used, with the inlet temperature maintained at 250°C in splitless mode. The oven temperature program began at 70°C, held for 1 minute, then increased to 260°C at 10°C/min, and finally held at 260°C for 5 minutes. The oven front inlet temperature was also set to 250°C. Helium was used as the carrier gas at a flow rate of 18 cm^3/min, a pressure of 4.9693 psi, and a septum purge flow of 3 mL/min. The ionization mode was set at 70 eV. Compound identification and quantitation were performed using Total Ion Count (TIC), and the mass spectra of the separated compounds were compared against the NIST02 Reference Spectral Library for identification.

3. Result and Discussion

3.1 Catalyst Characterization

The FT-IR spectrum of the synthesized (NiO/Al_2O_3) catalyst, displayed in Figure 2, reveals a vibrational peak characteristic of metal-oxygen stretching frequencies between 400 and 650 cm^{-1}. This range is consistent with the vibrations of Ni-O-Al-O and Ni-O-Al bonds, aligning with reported

findings (Aazza et al., 2020; El Nahrawy et al., 2020). A sharp peak observed around 469 cm^{-1} may correspond to the Ni-O stretching frequency of the functional group, possibly from nickel nitrate used in the synthesis. This further confirms the findings of Sokoto et al., (2017). The Ni-O peak intensity could have been reduced as nickel nitrate was decomposed to nickel oxide, as mentioned (Arranz & Palacio, 2023). Upon calcination, the nickel nitrate may have thermally decomposed into oxide and lost nitrate. Thus, this could lead to the loss of nitrate peak characteristics in the Infrared spectrum of the synthesized nickel oxide over alumina. The reduced intensity of the absorption band, which corresponds to nitrates, can be seen at 520 cm^{-1}, 500 $cm,^{-1}$ and 450 cm^{-1} on the IR spectrum of nitrate oxide from NiO/Al_2O_3. The absorption peak at 610 cm-1 in the infrared spectrum was due to Al-O stretching vibrations (Matsui et al., 2020). The observed characteristic absorption of NiO/Al_2O_3 aligns with the absorption previously reported for NiO/Al_2O_3 in reference (Alam et al., 2020).

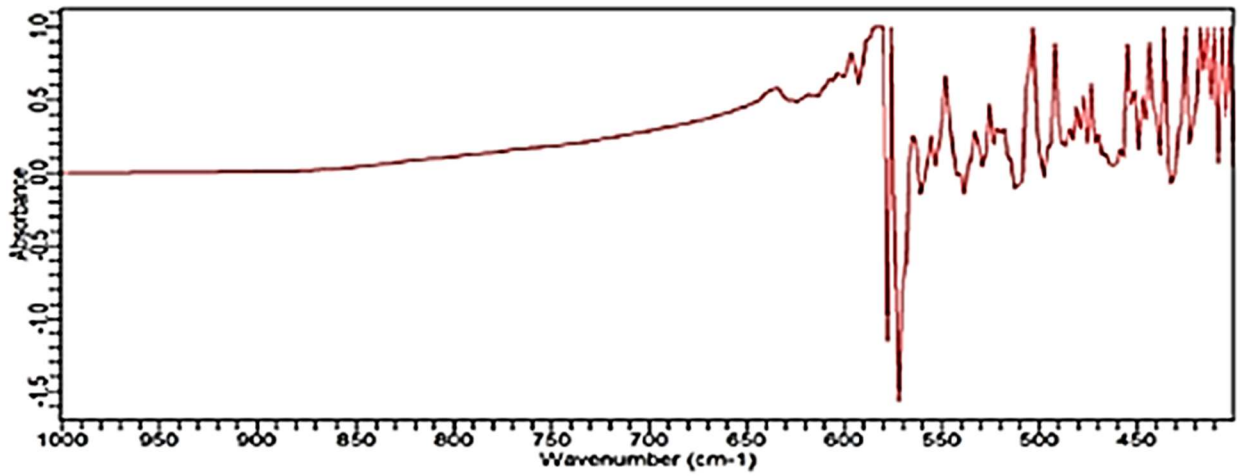

Figure 2: FT-IR Spectrum of the catalyst (NiO/Al_2O_3)

Figure 3 shows the XRD spectrum of the NiO Catalyst. The sharp, broad peaks observed in the XRD spectrum may be due to the medium-size effect and to combustion-related reflection peaks (Mlotswa et al., 2020). Incomplete combustion of the residue may have occurred during subsequent calcination at 600 °C, and pure cubic-phase NiO was obtained, as confirmed by (Cárdenas-Arenas et al., 2020). The calcined powder has crystallographic parameters in the Fm-3m space group (No. 225) and a lattice parameter of 4.178 Å. The calcined powder exhibits notable crystallographic features characteristic of a face-centered cubic (FCC) structure, as indicated by its assignment to the Fm-3m space group (space group number 225), which is consistent with the literature (Al-Hada et al., 2020; Das et al., 2021). The high symmetry inherent in the Fm-3m space group suggests that the material exhibits uniform, isotropic properties, which are advantageous for various applications, including catalysis and electronic devices. The lattice parameter of 4.178 Å (Devi et al., 2022) further underscores the unit cell's compact, orderly atomic arrangement. This structural uniformity may enhance the material's mechanical strength and thermal stability, making it suitable for high-temperature processes. Additionally, precise crystallographic information provides valuable insights into potential atomic-scale interactions, which can be crucial for tailoring the material's properties for specific applications.

https://doi.org/10.5281/zenodo.18727508

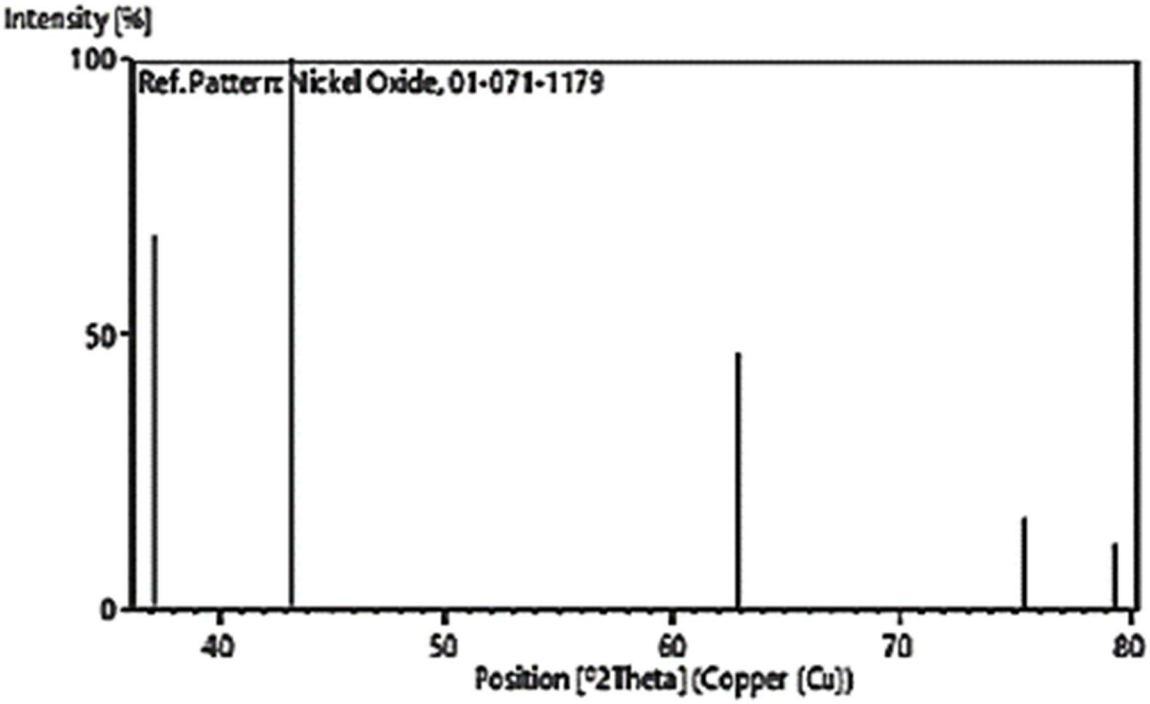

Figure 3: XRD spectrum of NiO Catalyst

Figure 4 shows the spectrum of the Al_2O_3 Catalyst. The XRD pattern shows sharp peaks indicating the presence of small-sized particles. The crystallographic parameters indicated a rhombohedral crystal system, space group R-3c (space group number 167), and lattice parameters a = b = 4.7590 Å and c = 12.9965 Å, as confirmed by the established findings (Mebed et al., 2022). This may be due to the high calcination temperature, which led to the formation of crystalline alpha-Al_2O_3 particles (Wang et al., 2021). The elemental analysis of the calcined powders also showed the absence of Ni, Al, and oxygen impurities (Mateos et al., 2019).

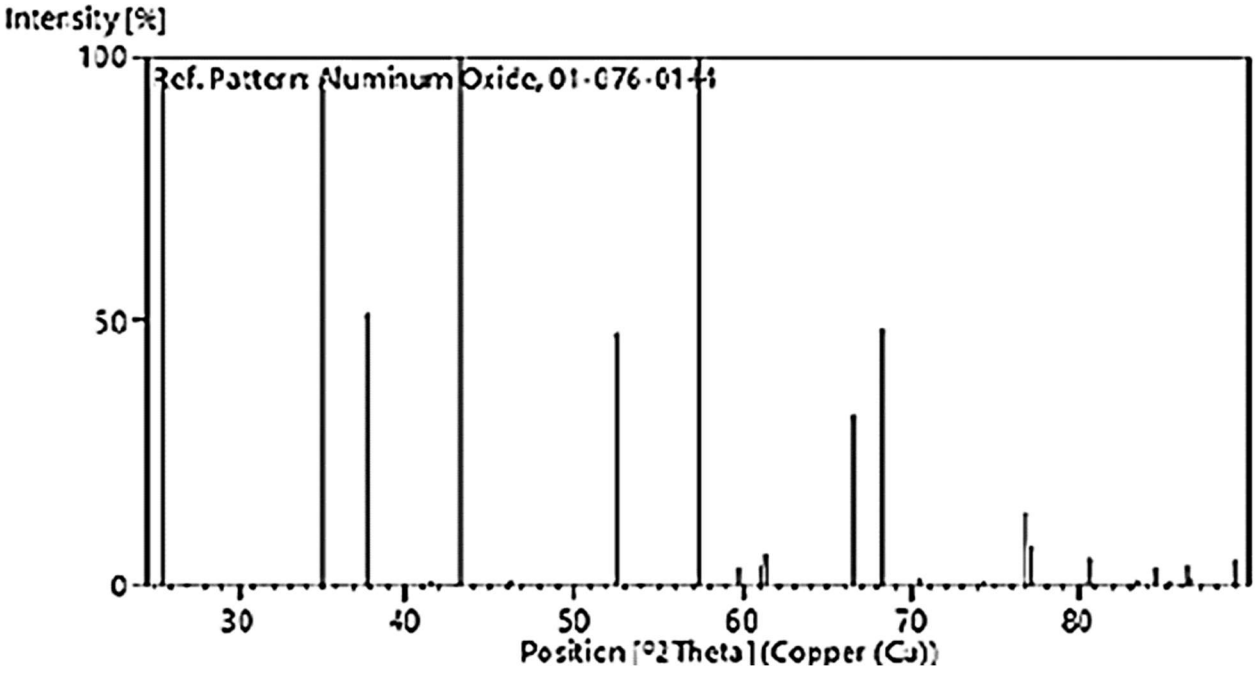

Figure 4: XRD Spectrum of Al_2O_3 catalyst support.

3.2 Proposed Reaction Mechanism and Catalyst Functionality

The conversion of hemicellulose derived from maize cobs into liquid hydrocarbons proceeds via a three-stage reaction pathway, comprising hydrolysis/dehydration, aldol condensation, and HDO.

Stage I: Acid-Catalyzed Hydrolysis and Dehydration

In the first stage, hemicellulose undergoes acid-catalyzed hydrolysis in the presence of sulfuric acid (H_2SO_4), yielding monomeric sugars, predominantly pentoses and hexoses. These sugars subsequently undergo acid-catalyzed dehydration to form furfural, a key intermediate.

$$\text{Hemicellulose} \xrightarrow{H_2SO_4} \text{Pentose/Hexoses}$$

$$C_5H_{10}O_5 + C_3H_6O \xrightarrow{-3H_2O} C_5H_4O_2 \text{ (Furfural)}$$

This step reduces oxygen content while generating a reactive platform molecule suitable for carbon–carbon coupling reactions.

Stage II: Base-Catalyzed Aldol Condensation

In the second stage, furfural undergoes aldol condensation with acetone in an alkaline medium (NaOH), forming a C_9 aldol adduct. This reaction effectively increases the carbon chain length, which is essential for producing hydrocarbons within the targeted fuel range (C_7–C_{15})

$$C_5H_4O_2 + C_3H_6O \xrightarrow{NaOH} C_9H_{10}O_3 + H_2O$$

The aldol condensation step represents a critical carbon-coupling route that bridges biomass-derived oxygenates to fuel-range intermediates.

Stage III: Hydrodeoxygenation and Hydrogenation

The aldol adduct is subsequently converted into linear alkanes (C_7–C_{15}) via hydrodeoxygenation and hydrogenation over a bifunctional NiO/Al_2O_3 catalyst at elevated temperature and hydrogen pressure.

$$C_9H_{10}O_3 + {}_xH_2 \xrightarrow{NiO/Al_2O_3} C_7\text{-}C_{15} \text{ alkane} + H_2O$$

This stage involves the simultaneous operation of two complementary catalytic functions.

Acidic Function (Al_2O_3)

The acidic sites on the alumina support promote deoxygenation reactions, including dehydration and

https://doi.org/10.5281/zenodo.18727508

decarbonylation, and facilitate further molecular rearrangements and condensation steps.

Metallic Function (NiO):

NiO serves as the primary active phase for hydrogenation and HDO reactions, enabling efficient cleavage of C–O bonds and saturation of C=C bonds. Catalyst characterization (Figure 3) confirms the presence of a cubic crystalline NiO phase, providing structurally uniform, catalytically accessible active sites. The compact atomic arrangement and high dispersion of NiO on the high-surface-area Al_2O_3 support ensure a high density of exposed metallic sites for effective hydrogen activation.

The synergistic interaction between acidic Al_2O_3 sites and metallic NiO centers underpins the catalyst's bifunctional nature, enabling efficient sequential dehydration, condensation, hydrogenation, and hydrodeoxygenation, ultimately yielding fuel-range hydrocarbons.

3.3 Identification of Furfural

The FT-IR assignment of functional groups to the produced furfural is shown in the Table 1.

Table 1: Spectral analysis of produced and standard furfural

Functional Group	Observed Frequencies cm^{-1}	Standard Furfural	Observed Furfural	Assignment
C=O	1780-1670	1988	1690	Aldehyde
C-H	2900-2700	2848-2814	2848-282	Aromatic
C-H	3100-3000	-	-	-
C=C	1600-1450	1570-1460	1570-1460	-
C-O	1300-1000	1200-1000	1200-1000	Ether

The FT-IR spectrum of the produced Furfural, shown in Figure 5, exhibited a strong and sharp absorption peak at 1690 cm^{-1}. This peak is characteristic of the conjugated carbonyl (C=O) group (Indriyanti et al., 2023). As indicated in Table 1, this C=O absorption frequency is lower than typically observed for aldehydes. This reduction is attributed to the internal hydrogen-bonding characteristic of conjugated unsaturated aldehydes and to the general effect of conjugation in lowering the carbonyl vibrational frequency (Cattaneo et al., 2021). A similar C=O absorption was also present in the standard furfural spectrum. Two weak absorptions confirmed the aldehyde functional group at 2848 cm-1 and 2812 cm-1 in the standard furfural spectrum. These correspond to the moderately intense aldehydic C-H stretching vibration. The observation of two peaks is due to Fermi resonance between the fundamental aldehydic C-H stretching vibration and its first overtone of the C-H bending vibration. Unlike the standard furfural spectrum, the produced furfural spectrum showed no peaks in the 2100 - 2260 cm-1 range. The peaks in this region of the standard spectrum may be due to other compounds in the commercial furfural standard (Chawananon et al., 2023). Both the produced and standard furfural spectra showed firm peaks between 1570 cm^{-1} and 1466 cm^{-1}, which are indicative of the C=C stretching vibrations within the aromatic ring. Additionally, a firm peak at 1020 cm^{-1} in both spectra confirmed the C-O stretching vibration. The spectrum also showed broad, lower absorptions at 3462 cm^{-1} and 3540 cm^{-1}. These peaks likely correspond to O-H vibrations and may be attributed to residual

solvent absorption in the product (Venzie et al., 2021). Hence, the IR spectrum of the produced furfural was consistent with that of the standard furfural spectrum.

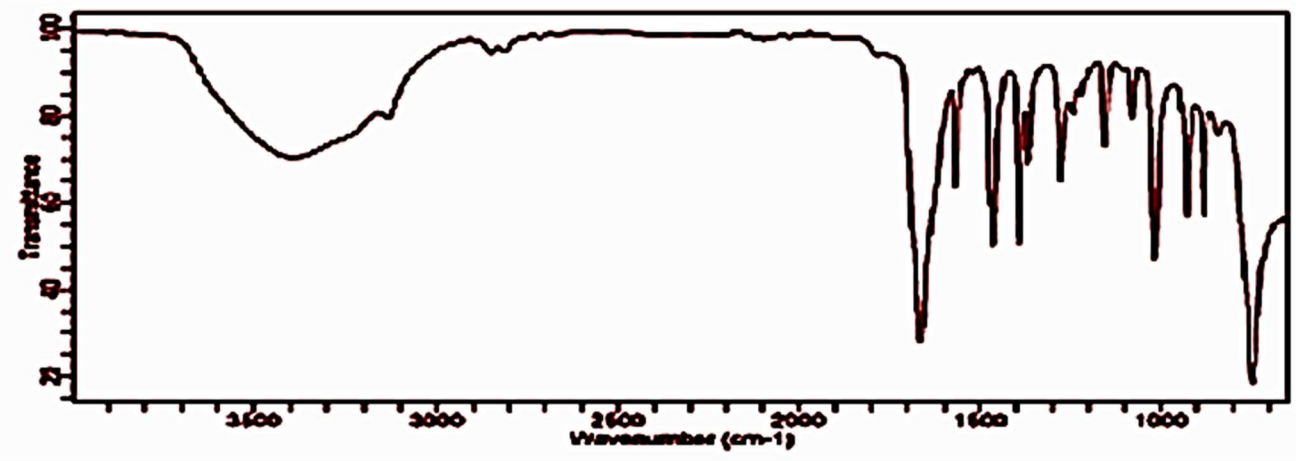

Figure 5: Furfural FT-IR Spectrum from Maize Cobs

3.4 Analysis of the Aldol Adducts

Table 2 shows the characteristics of aldol adducts as analyzed using FT-IR, from which the peak for each absorption was assigned.

Table 2: FT-IR Spectra of the Aldol Adducts

Class of Hydrocarbons	Functional Group	Wavenumber (cm-1)
Ketone	C=O	1700-1725
Alkenes Stretching	C-H	3080-3140
Alkenes	C=C	1630-1670
Aromatic	C-H	3000-3100
Aromatic	C-H	1450-1600
Ether	C-O	1199-1240

Figure 6 presents the FR-IR spectrum of the Furfural-Acetone dimer, with peak assignments listed in Table 2. The key absorption bands identified include (C–H) vibrational frequencies at 3055 and 3141 cm-1, which correspond to sp2 vibrations in the furan ring (Yamada & Mizuno, 2021). Infrared spectroscopy revealed several key functional groups. A stretching absorbance band at 1584 cm^{-1} suggests the presence of a carbonyl C=O group (Doney et al., 2020; Fuseya et al., 2020). The sharp stretching absorbances observed at 1199 cm^{-1} and 1240 cm^{-1} are likely attributable to the C-O stretching vibration characteristic of the cyclic C-O-C linkage found in furfural (Nejad et al., 2023). Additionally, broader, lower-frequency absorption bands at 3462 cm-1 and 3540 cm-1 may be due to O-H vibrations, possibly arising from residual solvent absorption in the product (Venzie et al., 2021).

https://doi.org/10.5281/zenodo.18727508

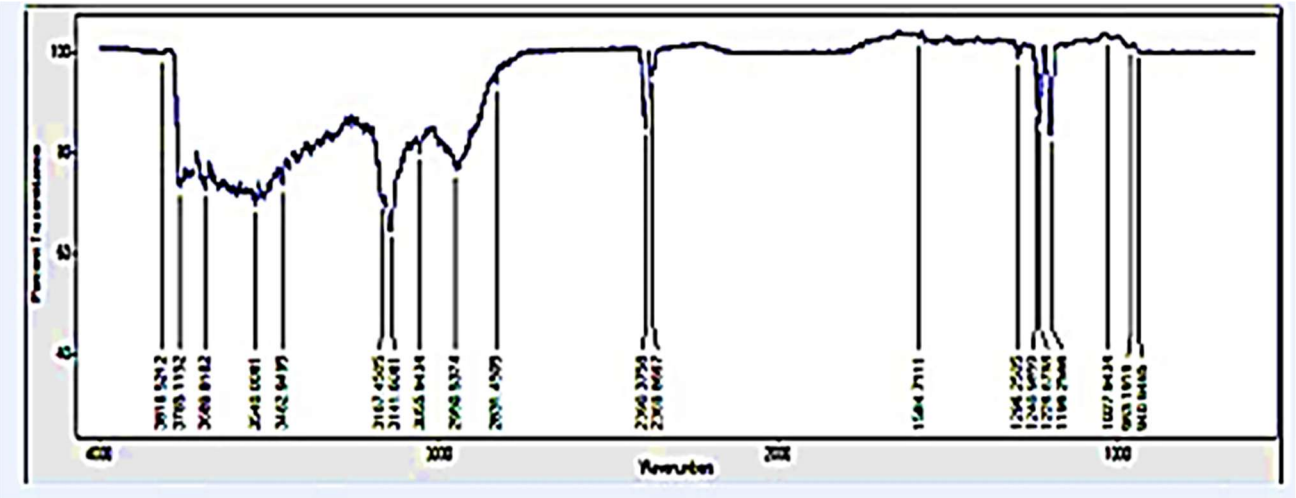

Figure 6: FT-IR Spectrum of the Aldol Adducts

3.5 Analysis of the Hydrodeoxygenation Products

Table 3 shows the chemical composition of hydrodeoxygenation products analyzed using GC-MS. The Table shows the distribution of hydrocarbons and oxygenates obtained from the hydrodeoxygenation of aldol adducts. The products were mainly liquid hydrocarbons within the carbon range of (C_5 - C_{20}). The presence of unsaturation (pentadecene) indicated partial hydrogenation, which might require further hydrogenation.

Table 3: Compositions of Hydrodeoxygenation Products

Component	Yield (%)	HC (%)
C_5-C_{10}	53.54	-
C_{11}-C_{20}	7.54	-
C_{20}+	-	-
Total	61.08	38.92
Oxygenates	-	-

The total relative peak area of hydrocarbons was 61.08%, with heptane and decane as the major products, each accounting for 28.06% and 17.65%, respectively. This result was higher than that reported for many catalysts in the literature (Table 4). In addition to alkanes, the liquid phase also contains substantial quantities of other alkanes, potentially resulting from decomposition and polymerization reactions. Other organic oxygenates, such as methanol and acetic acid, were found in the liquid phase but were not alkanes. These compounds are most likely byproducts of incomplete hydrogenation.

Table 4: Comparative performance of the developed catalyst and literature

Entries	Reference	Catalyst	Biomass	% Yield
1	Valizadeh, et al (2020)	Ni/Al_2O_3	Food waste	59.48
2	Melo, et al (2021)	$Mo\text{-}Co/\gamma\text{-}Al_2O_3$	waste cottonseed oil	61.90
3	Zheng, et al (2021)	$Pt\text{-}Ni/\text{-}Al_2O_3$	Pine sawdust	52.67
4	This work	NiO/Al_2O_3	Maize Cobs	61.08

This work makes a significant contribution by demonstrating the high efficiency of NiO/Al_2O_3 in converting maize cobs, an abundant agricultural waste, into valuable products. The comparable yield to the highest reported values underscores the potential of this catalyst-feedstock combination for sustainable and efficient waste-to-energy processes. This highlights the importance of exploring diverse feedstock and catalyst options to enhance the efficiency and sustainability of biomass conversion technologies.

4. Conclusion

This work successfully demonstrates the conversion of hemicellulose obtained from maize cobs into liquid hydrocarbons using NiO/Al_2O_3 as a bifunctional catalyst. The process achieved a high conversion rate of 61.08% under optimal conditions of 220°C, 30 bars, and 1 hour. GC-MS analysis revealed a significant yield of alkanes, particularly heptane and decane, underscoring the catalyst's efficiency in producing valuable liquid fuels. Compared with previous studies, including the 41.98% yield reported for NiO/SiO_2 using waste cooking oil, the catalyst exhibited superior performance. The IR spectrum and elemental analysis confirmed the structural integrity and purity of the synthesized catalyst. These results suggest that NiO/Al_2O_3 is a promising catalyst for sustainable biomass valorization, contributing to the development of advanced catalytic processes for renewable energy production. This study underscores the potential of utilizing maize cob-derived hemicellulose as a feedstock for liquid hydrocarbon production, thereby advancing the field of bio-based chemical synthesis.

Conflict of Interest

The authors affirm that they have no potential conflicts of interest, whether financial or personal, that could be interpreted as influencing the work presented in this paper.

Author Contributions

Gambo Muhammad: Led the manuscript writing, contributed to idea generation, and conducted the methodology development, experimentation, and data analysis.
M. N. Almustapha: Provided ideation, supervised the research process, and contributed to data analysis.
M. G. Liman: Contributed to ideation, supervised the study, and assisted in data analysis.
Abubakar Aji: Conducted data analyses, contributed to manuscript writing, and performed proofreading.
Hauwa Muhammad Abba: Assisted in manuscript writing and performed grammar checks.
Mysara Eissa Mohyaldinn: Supervised the research work.

Hisham Khaled Ben Mahmud: Supervised the research work.

Funding

No funding was received for the conduct of this study.

Acknowledgments

The authors acknowledge the support and guidance of their respective institutions and colleagues, who provided valuable insights during the preparation of this work. Special appreciation is extended to peers and mentors whose constructive feedback helped improve the manuscript's quality.

Ethical Statements

This study did not involve human participants, animals, or sensitive data requiring ethical approval. All procedures were conducted in accordance with relevant institutional and international guidelines. The authors affirm that the work complies with ethical standards for scholarly publishing.

Data and Code Availability

No code was involved in this study. All data supporting the findings are contained within the manuscript.

Supplementary Materials

All relevant materials are included within the manuscript; no additional supplementary files are provided.

References

Aazza, M., Ahlafi, H., Moussout, H., Mounir, C., Fadel, A., & Addad, A. (2020). Catalytic reduction of nitro-phenolic compounds over Ag, Ni and Co nanoparticles catalysts supported on γ-Al2O3. *Journal of Environmental Chemical Engineering*, *8*(2), 103707. https://doi.org/10.1016/j.jece.2020.103707

Aji, A., Mohyaldinn, M. E., & Mahmud, H. B. (2025a). The role of polymer nanocomposites in sustainable wax deposition control in crude oil systems—Systematic review. *AIMS Environmental Science*, *12*(1), 16–52. https://doi.org/10.3934/environsci.2025002

Aji, A., Mohyaldinn, M. E., & Mahmud, H. K. B. (2025b). Nature-driven synthesis of advanced eco-conscious Ag–ZnO nanomaterials: Mechanistic insights and breakthrough. *Proc IMechE Part N: J Nanomaterials, Nanoengineering and Nanosystems*. https://doi.org/DOI:%2010.1177/23977914251343683

Aji, U. A., Muhammad, C., Almustapha, M. N., Dandare, S. U., Zabi, A. M., Ntichika, V. C., Aliyu, A. A., & Gadzama, M. D. (2022). Catalytic Conversion of Furfural from Hemicellulose of Citru. *International Journal of Research and Innovation in Applied Science*, *7*(10). https://ideas.repec.org//a/bjf/journl/v7y2022i10p32-37.html

Alam, M. M., Rahman, M. M., Uddin, M. T., Asiri, A. M., Inamuddin, Saeed Chani, M. T., & Islam, M. A. (2020). Development of l-glutamic acid biosensor with ternary ZnO/NiO/Al2O3 nanoparticles. *Journal of Luminescence*, *227*, 117528. https://doi.org/10.1016/j.jlumin.2020.117528

Al-Hada, N., Kamari, H., Saleh, M., Flaifel, M. H., Al-Ghaili, A. M., Kasim, H., Baqer, A. A., Saion, E., & Jihua, W. (2020). Morphological, structural and optical behaviour of PVA capped binary (NiO)0.5 (Cr2O3)0.5 nanoparticles produced via single step based thermal technique. *Results in Physics*. https://doi.org/10.1016/j.rinp.2020.103059

Arranz, A., & Palacio, C. (2023). Influence of X Cation Covalence in the Formation of Ni-O-X Mixed Oxides by Reactive Ion Beam Mixing of Ni/X Interfaces. *Crystals*, *13*(2), 345. https://doi.org/10.3390/cryst13020345

Azman, N., Khairuddin, N., Azmi, T. S. M. T., Seenivasagam, S., & Hassan, M. A. (2023). Application of Biochar from Woodchip as Catalyst Support for Biodiesel Production. *Catalysts*. https://doi.org/10.3390/catal13030489

Azni, M. A., Khalid, R. M., Hasran, U. A., & Kamarudin, S. (2023). Review of the Effects of Fossil Fuels and the Need for a Hydrogen Fuel Cell Policy in Malaysia. *Sustainability*. https://doi.org/10.3390/su15054033

Boni, Y. M., Bouich, A., Oyedele, S. O., Messaoudi, N. E., Soucase, B. M., & Boko, A. (2023). Towards Electricity from the Combustion of Agricultural Waste in Boilers with Low CO_2 Emissions. *Sustainable Chemical Engineering*, 1–15. https://doi.org/10.37256/sce.5120243414

Cárdenas-Arenas, A., Quindimil, A., Davó-Quiñonero, A., Bailón-García, E., Lozano-Castelló, D., De-La-Torre, U., Pereda-Ayo, B., González-Marcos, J. A., González-Velasco, J. R., & Bueno-López, A. (2020). Isotopic and *in situ* DRIFTS study of the CO2 methanation mechanism using Ni/CeO2 and Ni/Al2O3 catalysts. *Applied Catalysis B: Environmental*, *265*, 118538. https://doi.org/10.1016/j.apcatb.2019.118538

Cattaneo, S., Capelli, S., Stucchi, M., Bossola, F., Santo, V. D., Araujo-Lopez, E., Sharapa, D. I., Studt, F., Villa, A., Chieregato, A., Vandegehuchte, B. D., & Prati, L. (2021). Discovering the role of substrate in aldehyde hydrogenation. *Journal of Catalysis*. https://doi.org/10.1016/J.JCAT.2021.05.012

Channi, H. (2022). *Energy Resources and Their Consumption* (pp. 267–276). https://doi.org/10.4018/978-1-7998-8561-0.ch013

Chawananon, S., Asselin, P., Claus, J. A., Goubet, M., Roucou, A., Georges, R., Sobczuk, J., Bracquart, C., Pirali, O., & Cuisset, A. (2023). Rovibrational Spectroscopy of Trans and Cis Conformers of 2-Furfural from High-Resolution Fourier Transform and QCL Infrared Measurements. *Molecules*, *28*(10). https://www.mdpi.com/1420-3049/28/10/4165

Chen, K., Rui, Z., Xu, C., & Huang, Z. (2023). The Conversion of Biowaste and Residue to Biofuel: From History, Physics Principles, to the Current Status of Technology, Mitigation of Environmental Impact and Economic Challenges. *Applied and Computational Engineering*, *7*, 822–835. https://doi.org/10.54254/2755-2721/7/20230565

Das, S., Nishad, S., & Robi, P. (2021). A New High-Entropy Alloy of Al–Fe–Co–Ni–Cu Possessing Single Face-Centered Cubic Crystal Structure and Excellent Mechanical Properties at Room Temperature. *Physica Status Solidi (a)*, *218*. https://doi.org/10.1002/pssa.202000825

Devi, P., Rohilla, S., Saini, J., & Patwa, R. (2022). Structural Characterization of Nanocomposites of NiO/H2O4Sn3 Prepared By Coprecipitation Method. *ECS Transactions*. https://doi.org/10.1149/10701.15291ecst

Doney, K., Kortyna, A., & Nesbitt, D. (2020). High-resolution infrared spectroscopy of HCF in the CH stretch region. *The Journal of Chemical Physics*, *152 1*. https://doi.org/10.1063/1.5133397

El Nahrawy, A. M., Elzwawy, A., Abou Hammad, A. B., & Mansour, A. M. (2020). Influence of NiO on structural, optical, and magnetic properties of Al_2O_3–P_2O_5–Na_2O magnetic porous nanocomposites nucleated by SiO_2. *Solid State Sciences*, *108*, 106454. https://doi.org/10.1016/j.solidstatesciences.2020.106454

Fuseya, G., Takeya, S., & Hachikubo, A. (2020). Effect of temperature and large guest molecules on the C–H symmetric stretching vibrational frequencies of methane in structure H and I clathrate hydrates. *RSC Advances*, *10*, 17473–17478. https://doi.org/10.1039/d0ra02748k

Garba, N. A., Muduru, I. K., Sokoto, M. A., & Dangoggo, S. M. (2018). *Production of Liquid Hydrocarbons From Millet Husk Via Catalytic Hydrodeoxygenation In NiO/Al_2 O_3 CATALYSTS*. 125–130. https://doi.org/10.2495/EQ180121

Halkos, G., & Gkampoura, E.-C. (2023). Assessing Fossil Fuels and Renewables' Impact on Energy Poverty Conditions in Europe. *Energies*. https://doi.org/10.3390/en16010560

Holechek, J. L., Geli, H. M. E., Sawalhah, M. N., & Valdez, R. (2022). A Global Assessment: Can Renewable Energy Replace Fossil Fuels by 2050? *Sustainability*, *14*(8), 4792. https://doi.org/10.3390/su14084792

Indriyanti, E., Adhityasmara, D., Praharsiwi, M. S., Wildan, A., Masduqi, A. F., Syukur, M., Mutiara, E., & Dinurrossifa, R. S. (2023). Potential Antioxidant Activity in Octyl p—Methoxycinnamate (OPMC) Compound Synthesized by Sonochemical Method. *Jurnal Akademika Kimia*. https://doi.org/10.22487/j24775185.2023.v12.i2.pp100-107

Inyang, V., Laseinde, O. T., & Kanakana, G. M. (2022). Techniques and applications of lignocellulose biomass sources as transport fuels and other bioproducts. *International Journal of Low-Carbon Technologies*, *17*, 900–909. https://doi.org/10.1093/ijlct/ctac068

Jiang, M., Tan, J.-B., Chen, Y., Zhang, W., Chen, P.-Q., Tang, Y.-C., & Gao, Q. (2023). Promoted electrocatalytic hydrogenation of furfural in a bi-phasic system. *Chemical Communications*. https://doi.org/10.1039/d3cc00051f

Kalak, T. (2023). Potential Use of Industrial Biomass Waste as a Sustainable Energy Source in the Future. *Energies*, *16*(4). https://www.mdpi.com/1996-1073/16/4/1783

Kandpal, R., & Singh, R. (2022). Renewable Energy Sources – A Review. *ECS Transactions*, *107*(1), 8133–8140. https://doi.org/10.1149/10701.8133ecst

Kashef, M., Attia, M., Kamh, M., & Abdel-Rahman, M. (2022). Techno-Economic Analysis of Renewable Energy Application in Oil and Gas Industry: A Case Study. *2022 23rd International Middle East Power Systems Conference (MEPCON)*, 1–6. https://doi.org/10.1109/MEPCON55441.2022.10021779

Mateos, D., Valdez, B., Castillo, J. R., Nedev, N., Curiel, M., Perez, O., Arias, A., & Tiznado, H. (2019). Synthesis of high purity nickel oxide by a modified sol-gel method. *Ceramics International*, *45*(9), 11403–11407. https://doi.org/10.1016/j.ceramint.2019.03.005

Mathew, S., Nagy, J. B., & N, N. (2023). Structure—Catalytic Activity Correlation in Aluminium Hydroxide Supported Vanadia Catalysts. *Proceeding International Conference on Science and Engineering*. https://doi.org/10.52783/cienceng.v11i1.156

Matsui, H., Shimatani, K., Ikemoto, Y., Sasaki, T., & Matsuo, Y. (2020). Phonon-assisted proton tunneling in the hydrogen-bonded dimeric selenates of Cs3H(SeO4)2. *The Journal of Chemical Physics*, *152 15*. https://doi.org/10.1063/1.5145108

Mebed, A. M., Abd-Elnaiem, A. M., Alshammari, A. H., Taha, T. A., Rashad, M., & Hamad, D. (2022). Controlling the Structural Properties and Optical Bandgap of PbO–Al2O3 Nanocomposites for Enhanced Photodegradation of Methylene Blue. *Catalysts*, *12*(2). https://www.mdpi.com/2073-4344/12/2/142

Melo, J. A., Sá, M. S. de, Moral, A., Bimbela, F., Gandía, L. M., & Wisniewski, A. (2021). Renewable Hydrocarbon Production from Waste Cottonseed Oil Pyrolysis and Catalytic Upgrading of Vapors with Mo-Co and Mo-Ni Catalysts Supported on γ-Al2O3. *Nanomaterials*, *11*. https://doi.org/10.3390/nano11071659

Mlotswa, D., Noto, L., Mofokeng, S., Obodo, K. O., Orante-Barrón, V. R., & Mothudi, B. (2020). Luminescence dynamics of MgGa2O4 prepared by solution combustion synthesis. *Optical Materials*, *109*. https://doi.org/10.1016/j.optmat.2020.110134

Mo, W., Ren, Y., Ma, Y., Guo, J., Feng, Z.-H., Zhang, S., & Yang, X.-Q. (2023). Structure Characteristics and Removal Behavior of the Deposited Carbon on Ni-Al2O3 Catalyst for CO2 Reforming of CH4. *Processes*. https://doi.org/10.3390/pr11102968

Nejad, A., Li, X., Zhu, T., Liu, Y.-I., & Duan, C. (2023). Mid-infrared Laser Spectroscopy of Jet-Cooled Formic Acid Trimer: Mode-Dependent Line Broadening in the C-O Stretching Region. *The Journal of Physical Chemistry Letters*, 7795–7801. https://doi.org/10.1021/acs.jpclett.3c01860

Nikolopoulos, I., Kogkos, G., Tsavatopoulou, V. D., Kordouli, E., Bourikas, K., Kordulis, C., & Lycourghiotis, A. (2023). Nickel—Alumina Catalysts for the Transformation of Vegetable Oils into Green Diesel: The Role of Preparation Method, Activation Temperature, and Reaction Conditions. *Nanomaterials*, *13*(3). https://www.mdpi.com/2079-4991/13/3/616

Qu, J., Lei, T., Sun, T., Wang, Z., & Chen, G. (2023). Exergy Analysis of Biomass-Based Ethyl Levulinate Fuel for Whole Life Cycle. *Journal of Biobased Materials and Bioenergy*, *17*, 105–113. https://doi.org/10.1166/jbmb.2023.2249

Sokoto, A., Kabir, I., Dangoggo, S. M., Anka, N., & Hassan, L. G. (2017). Optimization of furfural production from millet husk using response surface methodology. *Energy Sources, Part A: Recovery, Utilization, and Environmental Effects*, *40*, 1–5. https://doi.org/10.1080/15567036.2017.1405120

Valizadeh, S., Lam, S., Ko, C., Lee, S.-H., Farooq, A., Yu, Y. J., Jeon, J.-K., Jung, S.-C., Rhee, G., & Park, Y.-K. (2020). Biohydrogen production from catalytic conversion of food waste via steam and air gasification using eggshell- and homo-type Ni/Al2O3 catalysts. *Bioresource Technology*, *320 Pt B*. https://doi.org/10.1016/j.biortech.2020.124313

Venzie, A., Portoff, A., Fares, C., Stavola, M., Fowler, W. B., Ren, F., & Pearton, S. J. (2021). OH-Si complex in hydrogenated n-type β-Ga2O3:Si. *Applied Physics Letters*, *119*(6), 062109. https://doi.org/10.1063/5.0059769

Wang, Y., Lin, Q., Wang, C., Li, K., Sun, X., Song, X., Gao, Y., & Ning, P. (2021). Influence of drying and calcination temperatures for Ce-Cu-Al trimetallic composite catalyst on simultaneous removal H2S and PH3: Experimental and DFT studies. *Journal of Environmental Sciences*, *104*, 277–287. https://doi.org/10.1016/j.jes.2020.12.001

Yamada, T., & Mizuno, M. (2021). Infrared Spectroscopy in the Middle Frequency Range for Various Imidazolium Ionic Liquids—Common Spectroscopic Characteristics of Vibrational Modes with In-Plane +C(2)–H and +C(4,5)–H Bending Motions and Peak Splitting Behavior Due to Local Symmetry Breaking of Vibrational Modes of the Tetrafluorobo. *ACS Omega*, *6*, 1709–1717. https://doi.org/10.1021/acsomega.0c05769

Yurukcu, M., Yilmaz, K., Yondemli, H., & Oskay, M. (2023). Implementation of Renewable Technologies and Its Impact on Oil & Gas Resources Under Energy Market Dynamics Worldwide. *Day 4 Thu, May 25, 2023*. https://doi.org/10.2118/213034-ms

Zheng, Y., Wang, J., Li, D., Liu, C., Lu, Y., Lin, X., & Zheng, Z. (2021). Highly efficient catalytic pyrolysis of biomass vapors upgraded into jet fuel range hydrocarbon-rich bio-oil over a bimetallic Pt–Ni/γ-Al2O3 catalyst. *International Journal of Hydrogen Energy*. https://doi.org/10.1016/j.ijhydene.2021.06.082